Environment and Natural Resources Journal

Volume 25
Issue X
2027

Sorption Behavior and Removal Performance of Polypropylene Microplastics Using Bamboo Biochar and Rice Husk Ash in Aqueous Solution

Nantira Vorakarnchanabun[1], Suchanya Wongrod[1,2*], and Sasidhorn Buddhawong[1]

[1]Environmental Technology Program, School of Energy, Environment and Materials, King Mongkut's University of Technology Thonburi, Bangkok, Thailand
[2]Environmental and Energy Management for Community and Circular Economy (EEC&C) Research Group, King Mongkut's University of Technology Thonburi, Bangkok, Thailand

ARTICLE INFO

Received: 6 Apr 2026
Received in revised: 11 Aug 2026
Accepted: 24 Aug 2026
Published online: 10 Nov 2026
DOI: 10.32526/ennrj/25/20260136

Keywords:
Adsorption kinetics/ Adsorption isotherms/ Bamboo biochar/ Microplastics/ Polypropylene/ Rice husk ash/ Sorption

*** Corresponding author:**
E-mail:
suchanya.won@kmutt.ac.th

ABSTRACT

This study investigated the sorption behavior and removal efficiency of virgin polypropylene (PPV) and aged polypropylene (PPA) microplastics using bamboo biochar (BBC) and rice husk ash (RHA) in aqueous solution. The physicochemical properties and surface morphology of PPA, BBC, and RHA were characterized via scanning electron microscopy (SEM), Brunauer-Emmett-Teller (BET) surface area analysis, X-ray fluorescence (XRF), Fourier transform infrared (FTIR) spectroscopy, and X-ray diffraction (XRD). Furthermore, batch adsorption kinetic and isotherm experiments were conducted. The pH of the point of zero charge (pH_{pzc}) of PPV (5.45), BBC (8.05), and RHA (9.7) indicated that PPV surfaces show a net negative charge, whereas BBC and RHA exhibit net positive charges at neutral pH, promoting different electrostatic mechanisms between polypropylene microplastics and the adsorbents. PPA exhibited a higher removal efficiency than PPV, likely due to aging in surface water that induced surface modifications. Kinetic analysis revealed that PPV and PPA adsorption onto BBC follows a pseudo-second-order (PSO) model (R^2=0.887-0.944), suggesting chemisorption as the dominant mechanism, with similar rate constants (k_2=0.002 g/mg min). In contrast, PPV and PPA sorption by RHA was best described by a pseudo-first-order (PFO) model (R^2=0.876-0.966), indicating physisorption as the primary mechanism, with a higher kinetic rate for PPA (k_1=0.145 min^{-1}) compared to PPV (k_1=0.078 min^{-1}). Equilibrium was achieved within 24 h for both PPV and PPA. In addition, the adsorption isotherms of PPV and PPA on both BBC and RHA aligned well with the Freundlich model (R^2=0.984-0.993), indicating multilayer adsorption on heterogeneous surfaces. Overall, these findings demonstrate that BBC and RHA exhibit distinct sorption mechanisms toward polypropylene microplastics, with BBC favoring chemisorption and exhibiting a higher affinity for aged particles, while RHA primarily facilitates physisorption. Aging plays a key role in modifying microplastic surfaces, thereby enhancing the sorption behavior and removal performance.

HIGHLIGHTS

- Surface-water aging improved PPA removal by BBC, with limited effects on RHA.
- PPA showed faster PFO kinetics than PPV with RHA, but similar PSO kinetics with BBC.
- BBC favored chemisorption, while RHA exhibited physisorption.
- Freundlich isotherm best described PPV and PPA removal by both BBC and RHA.
- PPA showed lower Freundlich K_F values than PPV, indicating altered isotherm behavior.

1. INTRODUCTION

Microplastics, defined as plastic particles smaller than 5 mm, are currently recognized as one of the most prevalent contaminants in aquatic environments, displaying an ever-increasing presence (Yang et al., 2021). Their low density allows them to remain suspended or float, facilitating their widespread distribution in water systems (Naqash et

Citation: Vorakarnchanabun N, Wongrod S, Buddhawong S. Sorption behavior and removal performance of polypropylene microplastics using bamboo biochar and rice husk ash in aqueous solution. Environ. Nat. Resour. J. 2027;25(X):xx-xx.

al., 2020). Moreover, they can release toxic additives and act as carriers for hazardous substances, such as persistent organic pollutants, endocrine-disrupting chemicals, and heavy metals, posing significant risks to aquatic organisms and food webs (Amelia et al., 2021; Maocai et al., 2021; Vorakarnchanabun et al., 2026).

Adsorption has emerged as a promising and cost-effective approach for microplastic removal. In recent years, biochar derived from agricultural biomass has attracted attention, given its porous structure, high surface area, and abundant functional groups (Wang et al., 2020a).

Previous studies have demonstrated the increasing use of biomass-derived materials and industrial by-products, particularly bamboo biochar (BBC) and rice husk ash (RHA), as effective media for microplastic removal from water via multiple mechanisms. According to Wang et al. (2020b), biochar derived from corn straw and hardwood achieved high removal efficiencies (>90-95%) for polystyrene microplastic particles, primarily via filtration and physical immobilization mechanisms, including surface attachment, pore trapping, and entanglement. Similarly, Shi et al. (2023a) reported a removal efficiency of 67.4% for polystyrene using cetyltrimethylammonium bromide-modified magnetic biochar, where hydrophobic interactions and electrostatic adsorption were identified as the dominant mechanisms. In addition, ball-milled pinewood biochar has demonstrated an enhanced removal performance, achieving up to 95.2% removal of aminated polystyrene nanoplastics, given its increased surface area and surface reactivity (Shi et al., 2023b). Wu et al. (2022) reported that rice husk-derived magnetic biochar achieved removal efficiencies of up to 99.96% for microplastics under acidic conditions, where electrostatic interactions and reduced competition from anions contributed to the high removal efficiency. Furthermore, Bongchompho et al. (2024) observed that both bottom ash and fly ash exhibited higher removal efficiencies for polypropylene (PP) and polyethylene, particularly for smaller particle sizes (50-75 µm), highlighting the significant influence of particle size on adsorption behavior.

Nevertheless, despite such advances, several research gaps remain. Most previous studies have focused on a single type of biochar or microplastic, with limited comparative evaluations of biomass-derived adsorbents under similar conditions. Moreover, the effect of microplastic aging on adsorption behavior has not been systematically investigated. Environmental aging alters the surface properties of microplastics, which can significantly affect their adsorption behavior. Therefore, investigating aged microplastics is essential to better represent environmental conditions. Furthermore, research on the mechanisms governing the removal of virgin polypropylene (PPV) and aged polypropylene (PPA) microplastics, particularly using low-cost materials such as BBC and RHA, is limited. PP microplastics are among the most prevalent and persistent plastics in aquatic environments (Eriksen et al., 2014); thus, their removal via sustainable adsorbents is vital. Therefore, this study aimed to investigate the sorption behavior and removal performance of PPV and PPA using BBC and RHA in aqueous solution, focusing on the adsorption kinetics, isotherms, and underlying mechanisms.

2. METHODOLOGY

2.1 Materials and chemical reagents

In the presentation of PPV and PPA, PP powder (Merck Limited, Bangkok, Thailand) was first sieved to 0.05-0.30 mm using US standard mesh sieves (numbers 50 and 270). The PP was then aged with surface water for 0 and 3 weeks to obtain PPV and PPA, respectively. Aging was conducted at 30±2°C under UVA irradiation (320-360 nm, peak at 340 nm) using a 12 h light/12 h dark cycle and agitation at 200 rpm. After aging, the samples were rinsed with deionized (DI) water, dried at 60°C for 24 h, and stored in desiccators.

Regarding BBC and RHA, BBC was produced from bamboo (Nonthaburi, Thailand) via pyrolysis in a Japanese kiln (Iwate kiln) at 1,000°C for 15 days, while RHA was procured from a biomass power plant in Surin Province, Thailand, operating at 65 bar and 480°C. Both materials were sieved to 0.25-1.00 mm, washed with DI water to achieve a neutral pH, dried at 60°C for 24 h, and stored in desiccators prior to use.

Analytical-grade chemical reagents, including potassium nitrate (KNO_3, 0.1 M), nitric acid (HNO_3, 0.1 N), and sodium hydroxide (NaOH, 0.1 N), were used for solution preparation and pH adjustment.

2.2 Characterization of PP, BBC, and RHA

Surface morphologies and elemental compositions were analyzed using scanning electron microscopy with energy dispersive spectroscopy (SEM-EDS; Phenom ProX, Thermo Fisher Scientific, USA). The samples were mounted on carbon tape, sputter-coated with gold (20 mA, 1 min), and

examined at an accelerating voltage of 30 kV. The surface area, pore volume, and pore diameter were determined via the Brunauer-Emmett-Teller (BET) method (Autosorb iQ-C-AG, Quantachrome Instrument, USA) using N_2 adsorption-desorption analysis. Elemental compositions were determined via X-ray fluorescence (XRF) spectrometry (XUV 773, Fischer, Germany), and surface functional groups were characterized using Fourier transform infrared (FTIR) spectroscopy (Nicolet 6700, Thermo Scientific, USA) over a wave number range of 4,000-400 cm^{-1}, with 50 scans taken at a resolution of 2 cm^{-1}. Mineralogical compositions and crystallinities were determined via X-ray diffraction (XRD; Rigaku, Smart Lab SE, Japan) over a 2θ range of 5°-60°. These properties were then used to interpret the adsorption behavior of the materials.

2.3 pH at point of zero charge (pH_{pzc})

The pH_{pzc} of PPV, PPA, BBC, and RHA was determined using the solid addition method (Al-Maliky et al., 2021). A 0.1 M KNO_3 electrolyte solution (45 mL) was prepared, and the initial pH was adjusted to 2.0-12.0 using 0.1 N HNO_3 and/or 0.1 N NaOH before adjusting the final volume to 50 mL. Each sample (1 g) was then added to the solution, followed by agitation at 120 rpm for 48 h. The final pH was measured, and the pH_{pzc} was determined from the intersection of the initial and final pH curves (Khandaker et al., 2018; Jawad et al., 2020).

2.4 Adsorption kinetics and isotherms

Analysis of the adsorption kinetics of PPV and PPA using BBC and RHA was conducted in 1,000-mL volumetric flasks. Each solution contained 10 mg/L of PPV or PPA and an adsorbent dosage (BBC or RHA) of 4 g/L. The experiments were performed at 150 rpm and 30±2°C, with an initial pH of 7.0±0.1. Further, all experiments were conducted in duplicate, and aliquots were collected at 0, 5, 15, 30, 60, 120, 480, 1,440, 2,880, and 4,320 min (Alavijeh et al., 2019).

The adsorption isotherms were evaluated using initial PPV and PPA concentrations ranging from 3 to 100 mg/L. Each 50-mL bottle contained 0.2 g of adsorbent (equivalent to 4 g/L), and the experimental conditions were maintained as described above. The equilibrium time obtained from the adsorption kinetic studies was used in the adsorption isotherm experiments.

The PP concentrations were analyzed using a gas chromatography-mass spectrometry (GC-MS) instrument (Clarus 690 coupled with Clarus SQ8T, PerkinElmer, USA) equipped with a headspace sampler. Separation was achieved on a capillary column (i.d.=0.25 mm, film thickness=0.25 µm), using helium at 1.5 mL/min as the carrier gas. The injector temperature was set to 250°C, and the oven temperature was programmed from 40°C (2 min) to 300°C (2 min), with a total run time of 30 min. The mass spectrometer was operated under electron ionization at 70 eV, with interface and source temperatures of 150 and 230°C, respectively. The headspace system (TurboMatrix 40) was operated at 200°C with a transfer line temperature of 210°C. The detected mass range was m/z=30-600 (Santos et al., 2023), and the characteristic PP fragment at m/z=111 (retention time=11.95-11.97 min) was used for quantification based on a five-point calibration curve. The adsorption kinetics were modeled using pseudo-first-order (PFO) and pseudo-second-order (PSO) models, while the adsorption isotherms were described using the Langmuir and Freundlich models to interpret the adsorption mechanisms, as given by Equations 1-4 in Table 1. The model parameters were determined via linear regression using Microsoft Excel, with R^2 used to evaluate the goodness of fit.

Table 1. Adsorption kinetics and isotherm model equations (Shafiq et al., 2021)

Model	Linear form	Non-linear form	
Kinetics			
PFO	$\log(q_e - q_t) = \log q_e - \frac{k_1}{2.303}t$	$q_t = q_e(1 - \exp(-k_1 t))$	(1)
PSO	$\frac{t}{q_t} = \frac{1}{k_2 q_e^2} + \frac{1}{q_e}t$	$q_t = \frac{q_e^2 k_2 t}{q_e k_2 t + 1}$	(2)
Isotherms			
Langmuir	$\frac{1}{q_e} = \frac{1}{q_m} + (\frac{1}{q_m K_L})\frac{1}{C_e}$	$q_e = \frac{q_m K_L C_e}{(1 + K_L C_e)}$	(3)
Freundlich	$\log q_e = \log K_F + \frac{1}{n}\log C_e$	$q_e = K_F C_e^{1/n}$	(4)

3. RESULTS AND DISCUSSION

3.1 Material characterization

Figures 1(a) and 1(b) show SEM images of PPV and PPA, respectively, which exhibit particle sizes of 100-200 µm. The SEM images in Figures 1(c) and 1(d) reveal that BBC and RHA exhibit irregular and highly porous surface morphologies, with mesopores structures (2-50 nm) (Table 2), and honeycomb-like and cylindrical configurations (Farhana et al., 2018). These structural features are typically associated with high surface areas and pore volumes, which are advantageous for adsorption processes.

Table 2 presents the physicochemical characteristics of PPV, BBC, and RHA. PPV exhibits the lowest specific surface area (2.42 m^2/g), with a negligible pore volume (0.0005 cm^3/g) and an average pore diameter of 0.8113 nm, indicating a predominantly microporous structure (<2 nm) with limited active sites. BBC displays the highest surface area (136.02 m^2/g) and pore volume (0.0387 cm^3/g), with a larger average pore diameter (4.7543 nm), suggesting a well-developed mesoporous structure (2-50 nm). RHA also exhibits a relatively high surface area (103.05 m^2/g) and pore volume (0.0374 cm^3/g), with an average pore diameter of 2.5903 nm, indicating its porous structure. The pore size distribution analysis confirmed that BBC and RHA are predominantly mesoporous materials (2-50 nm), whereas PPV is largely microporous (<2 nm; Leng et al., 2021; Fahmi et al., 2018). The higher surface area and well-developed porosity of BBC and RHA provide abundant active sites and promote physical entrapment and surface interactions, thereby enhancing the adsorption performance (Elnour et al., 2019; Leng et al., 2021; Wang et al., 2020a).

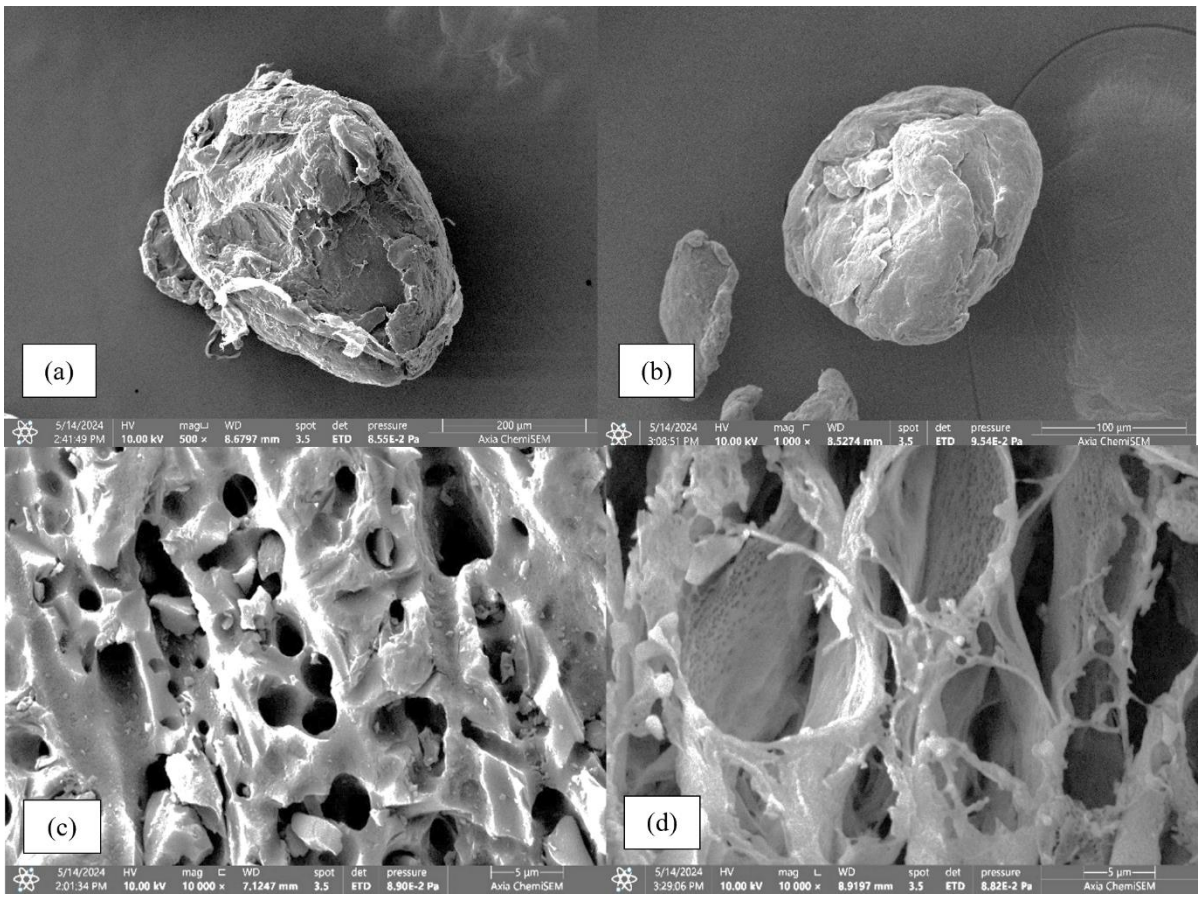


Figure 1. SEM analysis of (a) PPV, (b) PPA, (c) BBC, and (d) RHA

The XRF analysis revealed distinct mineral compositions, with BBC dominated by potassium oxide (K_2O) and RHA primarily composed of silicon dioxide (SiO_2), both of which influence the surface charge behavior and active site development (Rahmat, 2022). BBC provides heterogeneous and energetically favorable sites for PP adsorption via hydrophobic interactions, van der Waals forces, and electrostatic attraction, which are further enhanced by the aging-induced surface modifications of PP (Huang et al.,

2024). In contrast, RHA shows fewer reactive sites; thus, adsorption is mainly governed by physical entrapment and weaker surface interactions. Figure 2 presents the FTIR spectra of BBC and RHA, revealing oxygen-containing functional groups, including the disappearance of broad O-H stretching bands and the presence of a characteristic Si-O-Si peak for RHA. These mineral components may support surface interactions and adsorption processes (Li et al., 2021).

Table 2. Physical and chemical properties of PPV, BBC, and RHA

Properties	PPV	BBC	RHA
BET surface area (m^2/g)	2.42	136.02	103.05
Pore volume (cm^3/g)	0.0005	0.0387	0.0374
Adsorption average pore diameter (nm)	0.8113	4.7543	2.5903
XRF composition (wt.%)			
Silicon dioxide (SiO_2)	6.51	4.42	83.50
Potassium oxide (K_2O)	-	67.7	5.44
Calcium oxide (CaO)	8.37	8.33	3.46
Phosphorus pentoxide (P_2O_5)	10.70	3.78	2.66
Aluminum oxide (Al_2O_3)	6.95	0.47	0.89
Iron oxide (Fe_2O_3)	10.6	1.31	0.50
Copper(II) oxide (CuO)	4.74	0.54	0.01

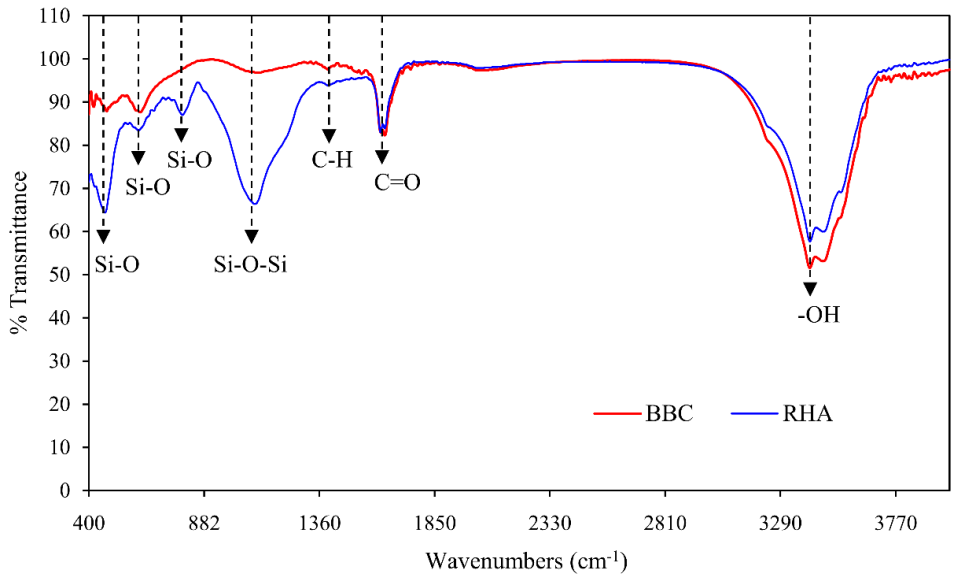


Figure 2. FTIR spectra of BBC and RHA

BBC (Figure 3(a)) exhibits a predominantly amorphous carbon structure with embedded crystalline mineral phases, including quartz (SiO_2) and calcite ($CaCO_3$). The amorphous carbon structure may provide abundant reactive surface sites that contribute to adsorption (Xiao et al., 2018; Chen et al., 2018). In contrast, RHA (Figure 3(b)) displays sharp and intense peaks dominated by crystalline SiO_2, reflecting a higher degree of crystallinity. The amorphous carbon matrix of BBC provides more chemically active sites; on the other hand, the crystalline structure of RHA is more rigid but offers fewer reactive sites. Similar observations have been made in previous studies, with carbon-rich biochars exhibiting an enhanced adsorption performance due to abundant surface defects and functional groups (Meng et al., 2024; Bolan et al., 2023).

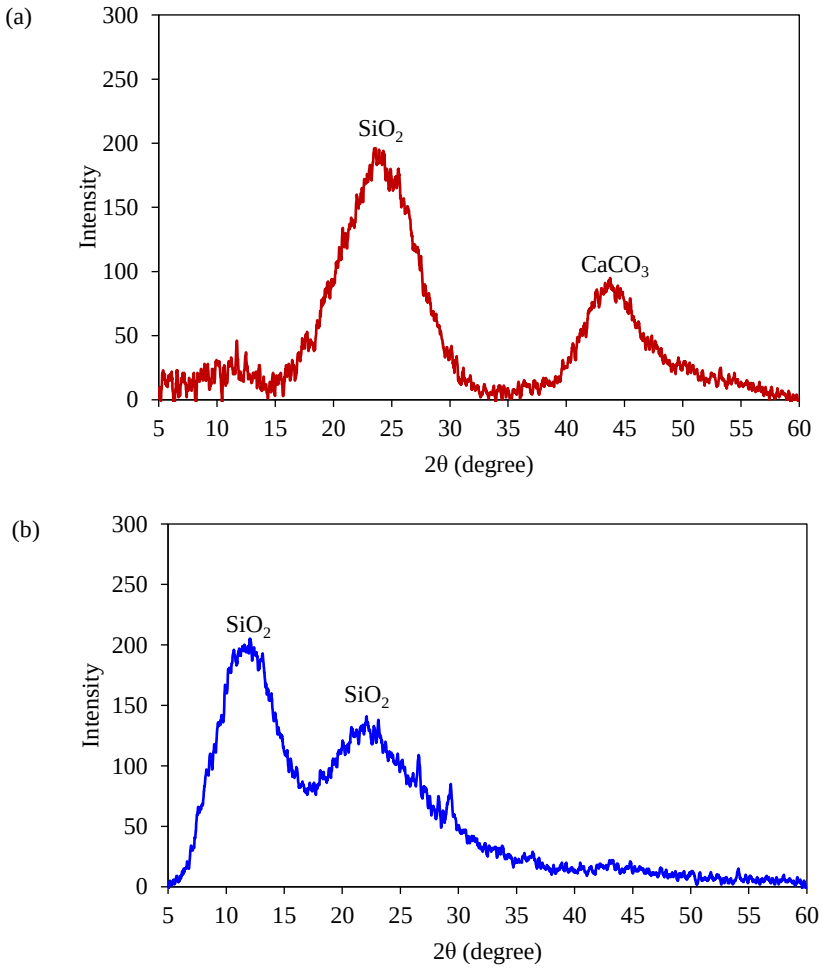


Figure 3. XRD analysis of (a) BBC and (b) RHA

These compositional and functional properties suggest that BBC and RHA possess abundant surface active sites that enhance their affinity for hydrophobic PP microplastics. Oxygen-containing functional groups promote hydrogen bonding and van der Waals interactions (Ji et al., 2024), while silica- and metal-containing mineral phases increase the surface heterogeneity and facilitate microplastic attachment via electrostatic and hydrophobic interactions (Gole et al., 2024). The combined presence of oxygenated functional groups, alkali and alkaline earth metals, and silica-rich mineral phases, as confirmed by XRF and FTIR spectroscopy, plays a crucial role in PP adsorption onto BBC and RHA in aquatic systems. The mesoporous structure and high surface area of BBC further enhance the adsorption capacity, while the fibrous and mineral-rich surface of RHA contributes via mechanisms such as physical entrapment, van der Waals forces, hydrophobic interactions, and surface adhesion (Elnour et al., 2019; Li et al., 2024; Gole et al., 2024; Dang et al., 2025). Studies have reported that environmental aging introduces oxygen-containing functional groups onto PP surfaces, thereby increasing their surface reactivity (Bhagat et al., 2022). These surface modifications may promote stronger interactions with the oxygen-containing active sites of BBC via hydrogen bonding and van der Waals interactions, which may explain the higher adsorption affinity of PPA observed in this study (Ji et al., 2024).

As shown in Figure 4, the pH_{pzc} values obtained for PPV, PPA, BBC, and RHA are 5.45, 4.9, 8.05, and 9.7, respectively, indicating distinct surface charge behaviors consistent with previous studies. BBC typically exhibits pH_{pzc} values of 7.2-8.3 due to its alkaline surface (Elnour et al., 2019), while untreated RHA typically shows higher pH_{pzc} values around 9.5-9.8, associated with its silica-rich composition and alkaline oxides (Li et al., 2024). In contrast, PPV usually exhibits lower pH_{pzc} values, commonly reported as falling between 4.2 and 4.6 (Liu et al., 2021), indicating a negatively charged surface under neutral pH conditions.

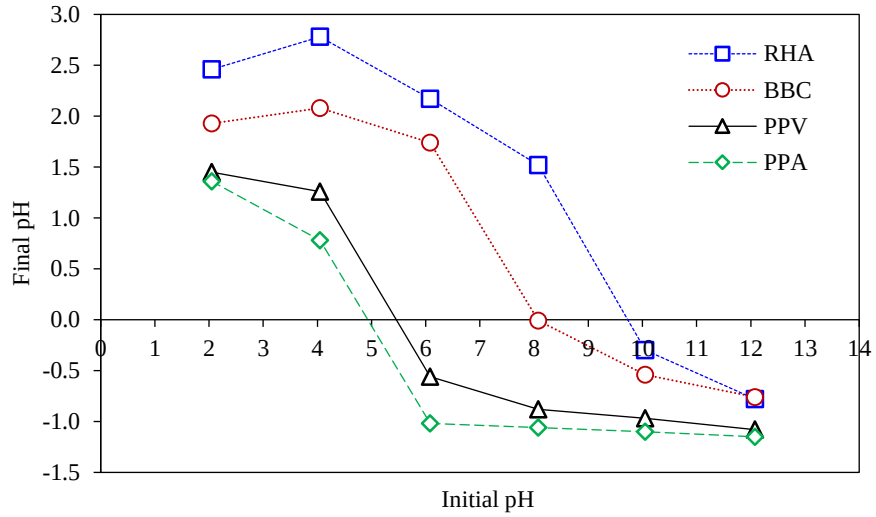


Figure 4. pH of point of zero charge (pH_{pzc}) of PPV, PPA, BBC, and RHA

These differences suggest that at neutral pH, PPV and PPA surfaces are negatively charged while BBC and RHA are positively charged, promoting electrostatic attraction and enhancing PP adsorption. Similar interactions have been reported as key mechanisms in microplastic-biochar systems (Kumar et al., 2023). The relatively high pH_{pzc} values, combined with the porous structure and high surface area of BBC and RHA, contribute to an improved adsorption performance.

3.2 Adsorption kinetics and isotherms

3.2.1 Adsorption kinetics

The adsorption kinetics were investigated to assess the effect of contact time on PPV and PPA sorption onto BBC and RHA, fitting PFO and PSO models to the kinetic data (Tables 3 and 4).

Table 3. Adsorption kinetics rate constants of PFO and PSO models for PPV and PPA adsorption by BBC

Model		PPV	PPA
PFO	k_1 (min^{-1})	0.125	0.066
	Q_e (mg/g)	38.45	48.45
	R^2	0.876	0.906
PSO	k_2 (g/mg min)	0.002	0.002
	Q_e (mg/g)	63.96	70.40
	R^2	0.887	0.944

Table 4. Adsorption kinetics rate constants of PFO and PSO models for PPV and PPA adsorption by RHA

Model		PPV	PPA
PFO	k_1 (min^{-1})	0.078	0.145
	Q_e (mg/g)	34.56	34.56
	R^2	0.876	0.966
PSO	k_2 (g/mg min)	0.002	0.003
	Q_e (mg/g)	54.14	44.45
	R^2	0.807	0.937

The kinetic analysis revealed the distinct adsorption behaviors of PP on BBC and RHA, (Figure 5). Adsorption on RHA is best described by the PFO model, particularly regarding the adsorption of PPA (R^2=0.966), indicating that physisorption dominates the process. Similar equilibrium adsorption capacities (Q_e=34.56 mg/g) for PPV and PPA suggest that polymer aging has a limited influence on PP uptake by RHA. This behavior is consistent with previous studies reporting that silica-rich materials tend to follow PFO

kinetics, where adsorption is governed by surface diffusion and weak physical interactions rather than chemical bonding (Nandiyanto et al., 2024). In contrast, adsorption on BBC follows the PSO model, with PPA adsorption showing a higher R^2 value (0.944) and greater Q_e (70.40 mg/g) than PPV adsorption (63.96 mg/g); this demonstrates that aging enhances PP adsorption on BBC. These findings agree with previous studies indicating that microplastic adsorption onto biochar is typically better described by PSO models, reflecting chemisorption and surface-controlled processes being driven by functional groups, active sites, and micropore-driven mass transfer (Dang et al., 2025; Cairns et al., 2024). Similar trends have also been reported for carbonaceous adsorbents, where a higher surface reactivity promotes stronger interactions with polymer surfaces (Wu et al., 2023).

The rate constant analysis further supports these trends. For RHA, PPA shows a higher k_1 than PPV, indicating a faster initial uptake without a significant increase in the adsorption capacity; this is characteristic of physisorption-controlled systems. Regarding BBC, a higher k_2 for PPA confirms that aging improves both the adsorption rate and capacity. These results highlight that PP adsorption on RHA is dominated by physisorption with a low sensitivity to aging, whereas BBC benefits significantly from polymer aging due to its chemically active surface (Bhagat et al., 2022).

The greater sorption affinity of PPA compared with PPV observed herein is consistent with previous evidence indicating that environmental aging enhances the abundance of oxygen-containing functional groups and increases surface polarity (Mohsenzadeh et al., 2025; Liang et al., 2023). These physicochemical changes promote stronger intermolecular interactions, such as hydrogen bonding, electrostatic attraction, and van der Waals forces, thereby enhancing the adsorption capacity. Comparable enhancements in the adsorption performance following polymer aging have also been reported for the interactions of polyethylene and polystyrene microplastics with biochar and other carbon-based materials (Wang et al., 2020a; Wu et al., 2023).

BBC exhibits higher adsorption capacities than RHA, which can be attributed to its larger surface area, well-developed mesoporous structure, and richer surface functional groups. In contrast, the stronger PFO model fitting for RHA suggests that physisorption is dominant due to its more limited functional groups and pore accessibility, similar to other silica-rich adsorbents (Nandiyanto et al., 2024).

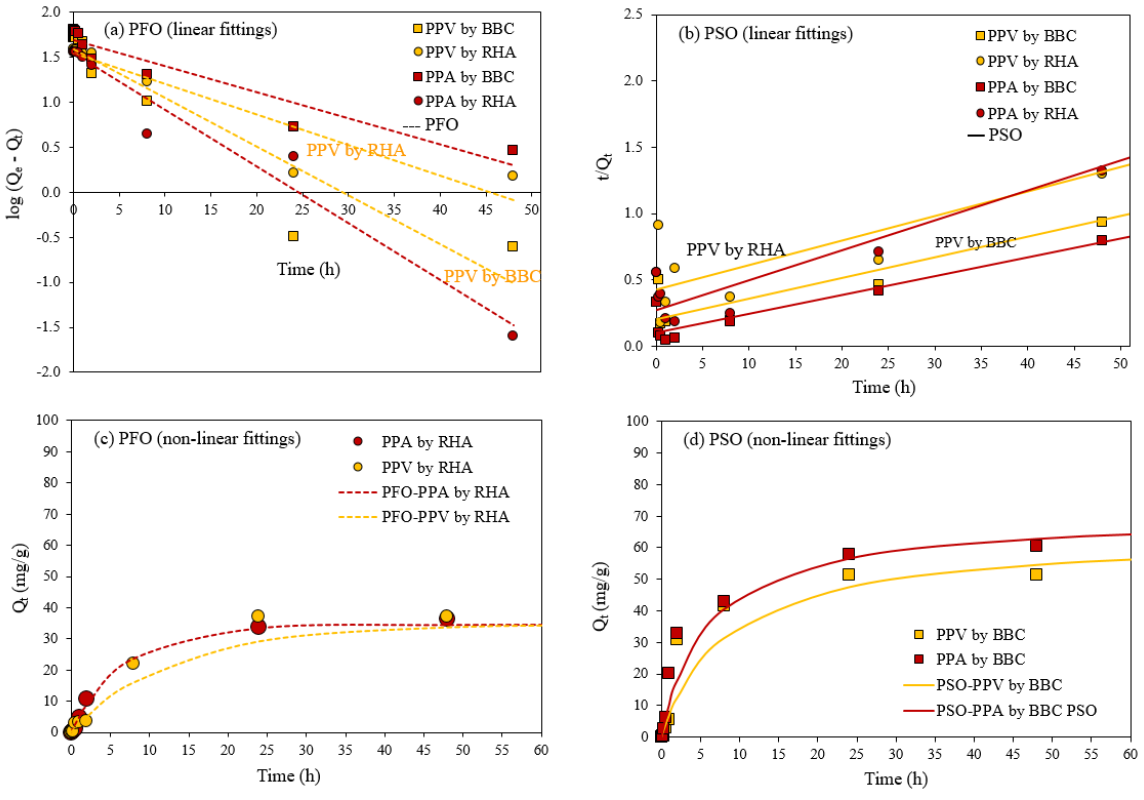


Figure 5. Linear fittings of (a) PFO and (b) PSO kinetic models and nonlinear fittings of (c) PFO and (d) PSO models for PPV and PPA adsorption on BBC and RHA

3.2.2 Adsorption isotherms

The adsorption isotherms were analyzed to describe the equilibrium sorption behavior of PPV and PPA on BBC and RHA. The Langmuir and Freundlich isotherm models were fitted to the experimental data, as show in Figure 6 and summarized in Tables 5 and 6.

The Langmuir maximum adsorption capacity (Q_m=26.946-29.09 mg/g) is highest for the BBC-PPA system, suggesting that BBC provides a greater density of energetically favorable sorption sites relative to RHA. The elevated Q_m value for BBC is consistent with its well-developed mesoporous structure and the presence of aromatic and oxygen-containing functional groups, which enhance hydrophobic and π-π interactions with the PP surfaces (Liu et al., 2021). The Langmuir constants (K_L=0.303-0.408 L/mg) further suggest a moderate to strong adsorption affinity, although with relatively lower R^2 values of 0.722-0.821; this implies that monolayer adsorption may occur, though other adsorption mechanisms may also contribute. Similar behavior has been reported for microplastic adsorption onto biochar and activated carbon materials, where the observed Langmuir fitting is often accompanied by additional mechanisms, such as pore filling and surface heterogeneity (Wu et al., 2023; Ji et al., 2024; Wang et al., 2020b).

Table 5. Adsorption isotherm parameters of the Langmuir and Freundlich models for PPV and PPA adsorption by BBC

Model		PPV	PPA
Langmuir	K_L (L/mg)	0.342	0.303
	Q_m (mg/g)	28.41	29.09
	R^2	0.738	0.722
Freundlich	K_F (mg/g (L/mg)$^{1/n}$)	6.112	5.810
	n	1.691	1.635
	R^2	0.990	0.993

Table 6. Adsorption isotherm parameters of the Langmuir and Freundlich models for PPV and PPA adsorption by RHA

Model		PPV	PPA
Langmuir	K_L (L/mg)	0.408	0.370
	Q_m (mg/g)	26.95	28.12
	R^2	0.809	0.821
Freundlich	K_F (mg/g (L/mg)$^{1/n}$)	6.416	6.294
	n	1.607	1.552
	R^2	0.984	0.989

The Freundlich adsorption constants (n=1.550-1.691) indicate favorable adsorption and suggest that the adsorption process occurs on heterogeneous surfaces. This is consistent with previous findings highlighting the tendency of microplastics to show multilayer accumulation on rough and chemically diverse biochar surfaces (Meng et al., 2024). BBC and RHA yield high K_F values of 5.81-6.416 mg/g (L/mg)$^{1/n}$, indicating their significant sorption capacity, given their porous structures and surface functional groups. The Freundlich model provides the best description of equilibrium behavior for both BBC and RHA (R^2=0.984-0.993), confirming that multilayer adsorption dominates the system. These results suggest that BBC and RHA possess heterogeneous surfaces with a wide distribution of adsorption energies. Similar behavior has been reported for biochar-based systems, where surface heterogeneity and pore complexity enhance the microplastic adsorption performance (Liu et al., 2021; Wu et al., 2023).

Notably, PPA exhibits a slightly higher adsorption capacity than PPV, particularly in the BBC system, indicating that polymer aging enhances the adsorption performance. This can be attributed to aging-induced surface oxidation; this increases the abundance of oxygen-containing functional groups and the surface polarity, promoting stronger intermolecular interactions, such as hydrogen bonding, electrostatic attraction, and van der Waals forces. Similar enhancements in the adsorption behavior of aged microplastics have been previously reported, where surface modification improves the

affinity toward carbonaceous adsorbents (Liang et al., 2023; Wang et al., 2020a).

Both the Langmuir and Freundlich isotherm models adequately describe the sorption behavior of PP onto BBC and RHA. However, the Freundlich model provides a better fit, indicating the dominance of heterogeneous and multilayer adsorption. The higher adsorption performance of BBC compared with RHA can be attributed to its higher surface area and larger pore volume (Table 2). This observation agrees with previous studies showing that the efficiency of adsorption is strongly governed by surface chemistry and pore accessibility, particularly for carbon-rich adsorbents, where hydrophobic and π-π interactions and binding to surface functional groups play key roles (Wang et al., 2020a; Wu et al., 2023). In contrast, the relatively lower performance of RHA suggests that silica-dominated materials show a greater reliance on weaker surface interactions, such as van der Waals forces and physical entrapment, due to limited active sites. Silica-based adsorbents exhibit similar behavior, where adsorption is mainly governed by physisorption and surface heterogeneity (Nandiyanto et al., 2024; Feng et al., 2025). These findings indicate that microplastic adsorption is controlled by the combined effects of surface functionality, pore structure, and interaction mechanisms.

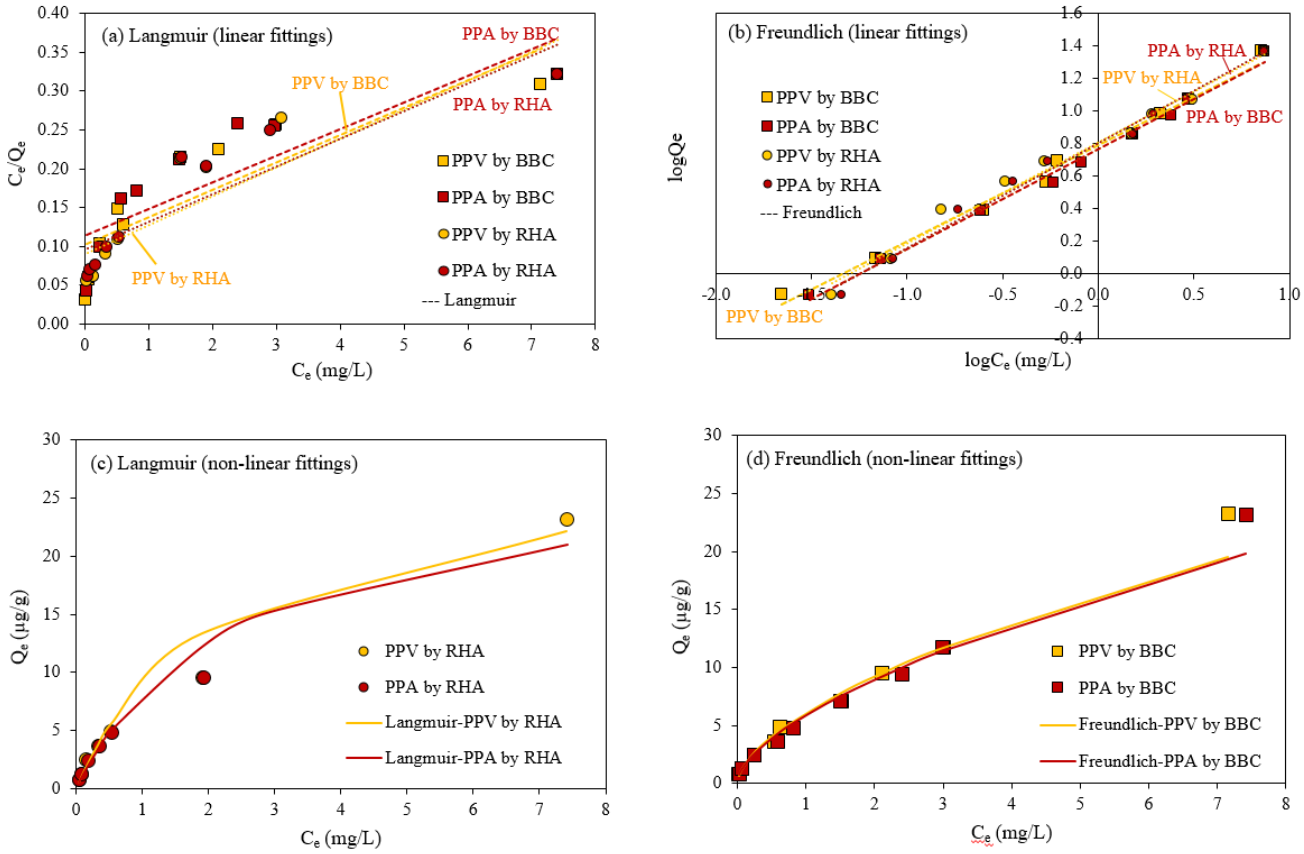


Figure 6. Linear fittings of (a) Langmuir and (b) Freundlich isotherm models and nonlinear fittings of (c) Langmuir and (d) Freundlich models for PPV and PPA adsorption on BBC and RHA

4. CONCLUSION

This study demonstrates that BBC and RHA exhibit distinct sorption behaviors toward PPV and PPA. The higher removal performance of PPA compared to PPV is attributed to surface oxidation, increased heterogeneity, and the presence of oxygen-containing functional groups, which enhance sorption interactions. The kinetic analysis revealed that adsorption onto BBC follows the PSO model, indicating chemisorption mechanisms involving surface complexation and interfacial interactions. On the other hand, adsorption onto RHA was better described by the PFO model, suggesting physisorption governed by its silica-rich composition and limited functional groups. The isotherm analysis showed that both the Langmuir and Freundlich models adequately describe the adsorption behavior, with the Freundlich model providing a better fit, indicating heterogeneous

and multilayer adsorption. BBC exhibited a higher adsorption capacity and affinity compared to RHA due to its well-developed pore structure and abundant surface functional groups.

Overall, BBC demonstrated a superior performance for microplastic removal, particularly for aged PP, while RHA showed a moderate performance dominated by physical interactions. These findings highlight the potential of agricultural waste-derived adsorbents for microplastic remediation. Future studies should focus on regeneration and long-term stability and performance under realistic environmental conditions to support large-scale applications.

ACKNOWLEDGEMENTS

The authors express their sincere gratitude to the Environment Technology Program, School of Energy, Environment and Materials (SEEM), for supporting this research. This work was supported by King Mongkut's University of Technology Thonburi (KMUTT), Thailand Science Research and Innovation (TSRI) and the National Science, Research and Innovation Fund (NSRF; fiscal year 2022, grant number FRB650048/0164) and the King Mongkut's University of Technology Thonburi fund (fiscal year 2020).

AUTHOR CONTRIBUTIONS

Conceptualization, N.V.; Investigation and Data Curation, N.V.; Formal Analysis, N.V.; Writing-Original Draft Preparation, N.V.; Supervision and Writing-Review and Editing, S.W.; Methodology and Validation, S.W.; Validation and Resources, S.B.; Project Administration, S.B.

DECLARATION OF CONFLICT OF INTEREST

The authors declare no conflicts of interest.

REFERENCES

Alavijeh MA, Sarvi MN, Afarani ZR. Modified montmorillonite nanolayers for nano-encapsulation of biomolecules. Heliyon 2019;5(3):e01379.

Al-Maliky EA, Gzar HA, Al-Azawy MG. Determination of point of zero charge (PZC) of concrete particles adsorbents. IOP Conference Series: Materials Science and Engineering 2021;1184(1):Article No. 012004.

Amelia TSM, Khalik WMAWM, Ong MC, Shao YT, Pan HJ, Bhubalan K. Marine microplastics as vectors of major ocean pollutants and its hazards to the marine ecosystem and humans. Progress in Earth and Planetary Science 2021;8:Article No. 12.

Bhagat K, Barrios AC, Rajwade K, Kumar A, Oswald J, Apul O, et al. Aging of microplastics increases their adsorption affinity towards organic contaminants. Chemosphere 2022;298: Article No. 134238.

Bolan N, Sarmah AK, Bordoloi S, Bolan S, Padhye LP, Zwieten LV, et al. Soil acidification and the liming potential of biochar. Environmental Pollution 2023;317:Article No. 120632.

Bongchompho W, Wongrod S, Chiarakorn S. Synergistic effect of microplastic type and particle size on microplastic removal from water using rice husk ash. Proceedings of the 13th International Conference on Environmental Engineering, Science and Management; 2024 May 9-10; Pullman Khon Kaen Raja Orchid, Khon Kaen: Thailand; 2024.

Cairns S, Meza-Rojas D, Holliman PJ, Robertson I. Interactions between biochar and nano(micro)plastics in the remediation of aqueous media. International Journal of Environmental Research 2024;18:Article No. 87.

Chen W, Wei R, Ni J, Yang L, Qian W, Yang Y. Sorption of chlorinated hydrocarbons to biochars in aqueous environment: Effects of the amorphous carbon structure of biochars and the molecular properties of adsorbates. Chemosphere 2018; 210:753-61.

Dang TMT, Huynh TTT, Chang-Chien GP, Bui HM. The role of biochar in combating microplastic pollution: A bibliometric analysis in environmental contexts. Beilstein Journal of Nanotechnology 2025;16:1401-16.

Elnour AY, Alghyamah AA, Shaikh HM, Poulose AM, Al-Zahrani SM, Anis A, et al. Effect of pyrolysis temperature on biochar microstructural evolution, physicochemical characteristics, and its influence on biochar/polypropylene composites. Applied Sciences 2019;9(6):Article No. 1149.

Eriksen M, Lebreton LC, Carson HS, Thiel M, Moore CJ, Borerro JC, et al. Plastic pollution in the world's oceans: More than 5 trillion plastic pieces weighing over 250,000 tons afloat at sea. PLoS One 2014;9(12):e111913.

Fahmi AH, Samsuri AW, Jol H, Singh D. Physical modification of biochar to expose the inner pores and their functional groups to enhance lead adsorption. RSC Advances 2018;8(67): 38270-80.

Farhana AN, Alias AB, Talib N, Rashid Z, Ghani WAWAK. Characteristics of rice husk biochar blended with coal fly ash for potential sorption material. Malaysian Journal of Analytical Sciences 2018;22(2):326-34.

Feng F, Wang S, He X, Wang X, Huang J, Liu G, et al. Adsorption behavior and mechanism of cadmium, copper, and lead on polylactic acid microplastics exposed to ultraviolet light. Journal of Environmental Chemical Engineering 2025; 13(3):Article No. 117033.

Gole P, Raut K, Kandasubramanian B. Polymer-based biochar materials for environmental remediation: A review. Hybrid Advances 2024;6:Article No. 100267.

Huang W, Jiang G, Xie L, Chen X, Zhang R, Fan X. Effect of oxygen-containing functional groups on the micromechanical behavior of biodegradable plastics and their formation of microplastics during aging. Journal of Hazardous Materials 2024;463:Article No. 132911.

Jawad AH, Malek NN, Abdulhameed AS, Razuan R. Synthesis of magnetic chitosan-fly ash/Fe_3O_4 composite for adsorption of reactive orange 16 dye: Optimization by Box-Behnken design. Journal of Polymers and the Environment 2020;28(3): 1068-82.

Ji G, Xing Y, You T. Biochar as adsorbents for environmental microplastics and nanoplastics removal. Journal of Environmental Chemical Engineering 2024;12(5):Article No. 113377.

Khandaker S, Toyohara Y, Kamida S, Kuba T. Adsorptive removal of cesium from aqueous solution using oxidized bamboo charcoal. Water Resources and Industry 2018;19:35-43.

Kumar R, Verma A, Rakib MRJ, Gupta PK, Sharma P, Garg A, et al. Adsorptive behavior of micro(nano)plastics through biochar: Co-existence, consequences, and challenges in contaminated ecosystems. Science of the Total Environment 2023;856:Article No. 159097.

Leng L, Xiong Q, Yang L, Li H, Zhou Y, Zhang W, et al. An overview on engineering the surface area and porosity of biochar. Science of the Total Environment 2021;763:Article No. 144204.

Li C, Huang Q, Zhang H, Wang Q, Xue R, Guo G, et al. Characterization of biochars produced by co-pyrolysis of Hami melon straw mixed with polypropylene and their adsorption properties of cadmium. International Journal of Environmental Research and Public Health 2021; 18(21):Article No. 11413.

Li W, Xing Y, Guo Y, Zhang D, Tang Y, Chen J, et al. The removal and mitigation effects of biochar on microplastics in water and soils: Application and mechanism analysis. Sustainability 2024;16(22):Article No. 9749.

Liang J, Wu J, Zeng Z, Li M, Liu W, Zhang T. Behavior and mechanisms of ciprofloxacin adsorption on aged polylactic acid and polyethylene microplastics. Environmental Science and Pollution Research 2023;30:62938-50.

Liu S, Shi J, Wang J, Dai Y, Li H, Li J, et al. Interactions between microplastics and heavy metals in aquatic environments: A review. Frontiers in Microbiology 2021;12:Article No. 652520.

Maocai S, Biao S, Guangming Z, Yaxin Z, Fengyun T, Chengyun Z. Surfactant changes lead adsorption behaviors and mechanisms on microplastics. Chemical Engineering Journal 2021;405:Article No. 126989.

Meng Z, Wu J, Huang S, Xin L, Zhao Q. Competitive adsorption behaviors and mechanisms of Cd, Ni, and Cu by biochar when coexisting with microplastics under single, binary, and ternary systems. Science of the Total Environment 2024;913:Article No. 169524.

Mohsenzadeh A, Persson M, Pettersson A, Frandsen FJ. Biochar for the removal of microplastics from water: A comprehensive scoping review. Microplastics 2025;4(4):Article No. 99.

Nandiyanto ABD, Nugraha WC, Yustia I, Ragadhita R, Fiandini M, Meirinawati H, et al. Isotherm and kinetic adsorption of rice husk particles as a model adsorbent for solving issues in the sustainable gold mining environment from mercury leaching. Journal of Mining Institute 2024;265:104-20.

Naqash N, Prakash S, Kapoor D, Singh R. Interaction of freshwater microplastics with biota and heavy metals: A review. Environmental Chemistry Letters 2020;18(6):1813-24.

Rahmat A. X-ray fluorescence analysis of *Aquilaria malaccensis* wood sawdust biochar prepared under low-temperature pyrolysis. Open Soil Science and Environment 2022;1(1):1-7.

Santos LHMLM, Insa S, Arxé M, Buttiglieri G, Rodríguez-Mozaz S, Barceló D. Analysis of microplastics in the environment: Identification and quantification using pyrolysis-GC/MS. MethodsX 2023;10:Article No. 102143.

Shafiq M, Alazba AA, Amin MT. Kinetic and isotherm studies of Ni^{2+} and Pb^{2+} adsorption from synthetic wastewater using *Eucalyptus camdulensis*-derived biochar. Sustainability 2021;13(7):Article No. 3785.

Shi Q, Guo S, Tang J, Lyu H, Ri C, Sun H. Enhanced removal of aged and differently functionalized polystyrene nanoplastics using ball-milled magnetic pinewood biochars. Environmental Pollution 2023a;316:Article No. 120696.

Shi Y, Du J, Zhao T, Feng B, Bian H, Shan S, et al. Removal of nanoplastics from aqueous solution by aggregation using reusable magnetic biochar modified with cetyltrimethyl-ammonium bromide. Environmental Pollution 2023b;318:Article No. 120897.

Vorakarnchanabun N, Wongrod S, Buddhawong S. Sorption behaviors and mechanisms of cadmium on polypropylene, bamboo biochar, and rice husk ash in aqueous solutions. Polish Journal of Environmental Studies 2026;35(5):5855-65.

Wang F, Zhang M, Sha W, Wang Y, Hao H, Dou Y, et al. Sorption behavior and mechanisms of organic contaminants to nano and microplastics. Molecules 2020a;25(8):Article No. 1827.

Wang Z, Sedighi M, Lea-Langton A. Filtration of microplastic spheres by biochar: Removal efficiency and immobilisation mechanisms. Water Research 2020b;184:Article No. 116165.

Wu J, Yang C, Zhao H, Shi J, Liu Z, Li C, et al. Efficient removal of microplastics from aqueous solution by a novel magnetic biochar: Performance, mechanism, and reusability. Environmental Science and Pollution Research 2023; 30:26914-28.

Xiao X, Chen B, Chen Z, Zhu L, Schnoor JL. Insight into multiple and multilevel structures of biochars and their potential environmental applications: A critical review. Environmental Science and Technology 2018;52(9):5027-47.

Yang L, Zhang Y, Kang S, Wang Z, Wu C. Microplastics in soil: A review on methods, occurrence, sources, and potential risk. Science of the Total Environment 2021;780:Article No. 146546.